Higher-order epistasis shapes natural variation in germ stem cell niche activity

Sarah R Fausett[1,#a,*], Asma Sandjak[1,2], Bénédicte Billard[1,2], & Christian Braendle[1*]

[1]Université Côte d'Azur, CNRS, Inserm, IBV, Nice, France
[#a]Department of Biology and Marine Biology, University of North Carolina Wilmington, Wilmington, NC, USA

[2]These authors contributed equally to this work

*Corresponding authors
Email: fausetts@uncw.edu
Email: braendle@unice.fr

Summary
Natural quantitative variation in developmental processes must be driven by allelic variation. Yet, the genotype-phenotype relationships underlying developmental system variation are understudied due to their inherent complexity. Taking advantage of the simple *Caenorhabditis elegans* germline stem cell system, we characterized natural differences in the germ stem cell niche activity of two distinct wild isolates—measured as differences in germline progenitor zone (PZ) size. Through quantitative trait locus (QTL) analysis, we detected multiple candidate causal loci, including two large-effect QTL on chromosomes II and V. Resolving the chromosome V QTL, we show that the isolate with a smaller PZ exhibits a unique 148 bp deletion in the promoter region of the Notch ligand, *lag-2*, a central signal promoting germ stem cell fate and proliferation. As predicted, introducing this deletion into the isolate with a large PZ resulted in a smaller PZ. Unexpectedly, re-introducing the deleted ancestral sequence in the isolate with a smaller PZ further reduced PZ size. Using allelic replacement lines, we show that these contradictory phenotypic effects are due to epistatic interactions among the *lag-2* promoter, the chromosome II QTL, and additional loci in the genome. Although the *lag-2* deletion appeared to explain natural variation in germ stem cell niche activity, its effects across multiple genetic backgrounds were unpredictable due to higher-order epistasis. Studying the genetic architecture of quantitative developmental systems without taking into account its natural variation may be misleading, emphasizing the need for a better integration of developmental and quantitative genetics.

Keywords
germ stem cell, QTL, natural variation, *C. elegans*, epistasis, evolution, Delta/Notch, proliferation, *lag-2*

Introduction

Fine-tuning of cellular proliferation is a fundamental aspect of organismal development and tissue homeostasis, often coordinated by stem cell niches. Even small perturbations in stem cell niche activity can deregulate tissue growth and maintenance to cause pathologies[1]. Dissecting the molecular genetic mechanisms regulating the activity of stem cell niches has, therefore, become a major focus of biological research. While developmental genetic studies of stem cell niche function in animals have unraveled underlying key molecular regulatory mechanisms, whether and how stem cell activity is modulated by genetic variation segregating in natural populations remains largely unaddressed. If it exists, how does such allelic variation contribute to variation in stem cell niche activity? Do known genes involved in stem cell niche signaling harbor this variation? And to what extent can natural variation in stem cell niche activity be explained by effects of single, large-effect genetic variants versus polygenic contributions of small-effect variants? Most quantitative traits are considered to be complex, involving a polygenic architecture, with genetic variants not only acting additively but also in an interactive manner. Such epistasis, also termed gene-gene (G x G) interactions, corresponds to non-additive interactions between allelic variants at different genomic loci[2]. Strong polygenicity and epistasis have been observed for most quantitative phenotypes across distant taxa[3–8] but detailed mechanistic dissection of complex epistatic interactions, including higher-order epistasis where three or more loci interact, remains rare[9–15]. Although experimentally difficult to characterize, molecular and quantitative genetic analyses also suggest that widespread epistatic interactions underlie developmental phenotypes[15,16,19,21,23,25,27,29,31,96]. Yet, so far, there is no information on how interactions among natural alleles cause quantitative variation in animal stem cell systems.

Germline stem cell (GSC) systems are fundamental to metazoan development and reproduction, maintaining immortal germ cell populations in an undifferentiated state and integrating genetic and environmental cues to adjust the production of germ cell progenitors[117,18]. Genetic research and comparative evo-devo studies have uncovered a diversity of GSC systems across distant taxa[20,22,24], but whether the activities of these systems show quantitative variation in natural populations of the same species is currently not known. Genomic and developmental genetic analysis of closely related species (e.g. within the genus *Drosophila* or the nematode genus *Caenorhabditis*) indicate that principal features, such as the key molecular signaling pathways and cell-cell interactions, of the GSC niche are largely conserved within genera[26,28,30,32,33]. Nevertheless, population-genetic studies in *Drosophila* show that central GSC genes can harbor surprisingly high levels of allelic variation, even within species, suggesting that these genes evolve rapidly and often due to positive selection[34–36]. Therefore, despite their importance in a fundamental developmental process, regulatory genes of GSC niches do not seem to be evolutionarily constrained. What remains unclear is how observed natural allelic variation translates into phenotypic variation in GSC niche activity.

To study the genetic basis of natural quantitative variation in GSC niche activity, we use the GSC system in *C. elegans*, which has served as a simple *in vivo* system to study stem cell niche function and involves a set of well-defined molecular signaling pathways[17,37,38]. The *C. elegans* hermaphrodite germline consists of two symmetrical arms with distal germ cell progenitor zones (PZ), also termed mitotic or proliferative zones, that include the stem cells, as well as progenitor cells in mitosis and meiotic S phase (Figure 1A). Germ cells differentiate into gamete progenitors through meiotic stages as they progress toward the proximal end of the arm (Figure 1A)[17,37]. The key regulatory signals are expressed by the Distal Tip Cell (DTC), a somatic gonadal cell that caps, and makes contact with, cells in the PZ (Figure 1A). These signals are the Delta/Serrate/LAG-2 (DSL-family) ligands, LAG-2 and APX-1, which activate Notch (GLP-1) receptors in distal germ cells, promoting the stem cell fate and inhibiting entry into meiosis[39–45]. The DTC with its contacts thus constitutes a stem cell niche[17]. GLP-1/Notch signaling is necessary and sufficient for the maintenance of the germ stem cell pool[17,38]. Germ cells progressively enter meiosis as they move proximally and lose contact with the DTC. This is controlled by a network

of RNA regulatory proteins, including PUF (Pumilio and FBF) RNA-binding proteins that promote self-renewal downstream GLP-1/Notch and other RNA regulatory proteins (GLD-1, GLD-2, SCF^{PROM-1}) that promote entry into meiosis[17,37,38,46–48]. Additional signals from gonadal sheath cells further modulate *C. elegans* germ cell proliferation and differentiation[49–55]. Germline PZ cell number is thus determined by the interplay of distal proliferative activity and the spatio-temporal transition into the proximal meiotic state. Moreover, proliferative activity of the *C. elegans* germline is highly sensitive to variation in physiology and the external environment, differing in response to nutrient quality and quantity, temperature, or social environment[17,30,56–60]. Environmental variation modulates GSC proliferation via metabolic and sensory signaling pathways (e.g., TGF-β, TOR, AMPK and insulin), which act both dependently and independently of niche-mediated Delta/Notch signaling[61–67]. The *C. elegans* germ stem cell system is thus highly plastic, capable of fine-tuning its activity in response to subtle environmental changes. Whether natural genetic variation can similarly modulate activity of this stem cell system is not known. However, previous reports suggest that the size of germline progenitor pool varies not only among different *Caenorhabditis* species but also among distinct *C. elegans* wild isolates[30,68].

In this study, we aimed to quantify and genetically characterize natural variation in *C. elegans* germ stem cell niche activity. We show that germline progenitor zone (PZ) size—here, a proxy for germ stem cell niche activity—differs between genetically and geographically distinct wild isolates under identical standard lab conditions. We used a QTL mapping approach to identify genomic regions associated with natural variation in PZ size, concentrating on two wild isolates with pronounced differences in PZ size. Genetic mapping revealed four candidate QTL including two large-effect loci on chromosomes II and V that act additively to explain ~32% of the variation in PZ size among the lines of the mapping set. We discovered that the QTL region on chromosome V harbors an INDEL variant in the promoter region of the DSL ligand *lag-2*, which causally contributes to variation in PZ size. However, we also discovered that the phenotypic effects of this variant are strongly modulated through epistatic interactions with the QTL on chromosome II and additional, unknown genomic loci. Taken together, our results indicate that complex epistatic interactions are important contributors to natural variation in germ stem cell niche activity and provide first insights into the quantitative genetic architecture of an animal stem cell system.

RESULTS

Germline progenitor zone size varies among natural *Caenorhabditis* populations.

Under standard laboratory conditions, the hermaphrodite germline progenitor zone (PZ) of the reference wildtype *C. elegans* strain (N2) typically contains ~250 cells during early adulthood[17]. Imaging through the entire PZ and counting the total number of germ cells is time-consuming and inefficient for screening large numbers of strains. To quantify natural variation in PZ size among many wild isolates of *Caenorhabditis*, we first developed a method to approximate PZ size by quantifying the trans-sectional area of the PZ in a single fluorescent image of a whole-mount DAPI-stained gonad (Figure 1B). PZ measurements derived by this method correlated well with individual counts of PZ nuclei from image stacks through the entire PZ (adj. $R^2 = 0.758$, $p<2.2e-16$) (Figure 1C, Table S1). We examined several wild isolates of *C. elegans* and *C. briggsae* from around the globe and discovered significant inter- and intraspecific variation in PZ size when measured in standard lab conditions (Figure 1D, Table S2).

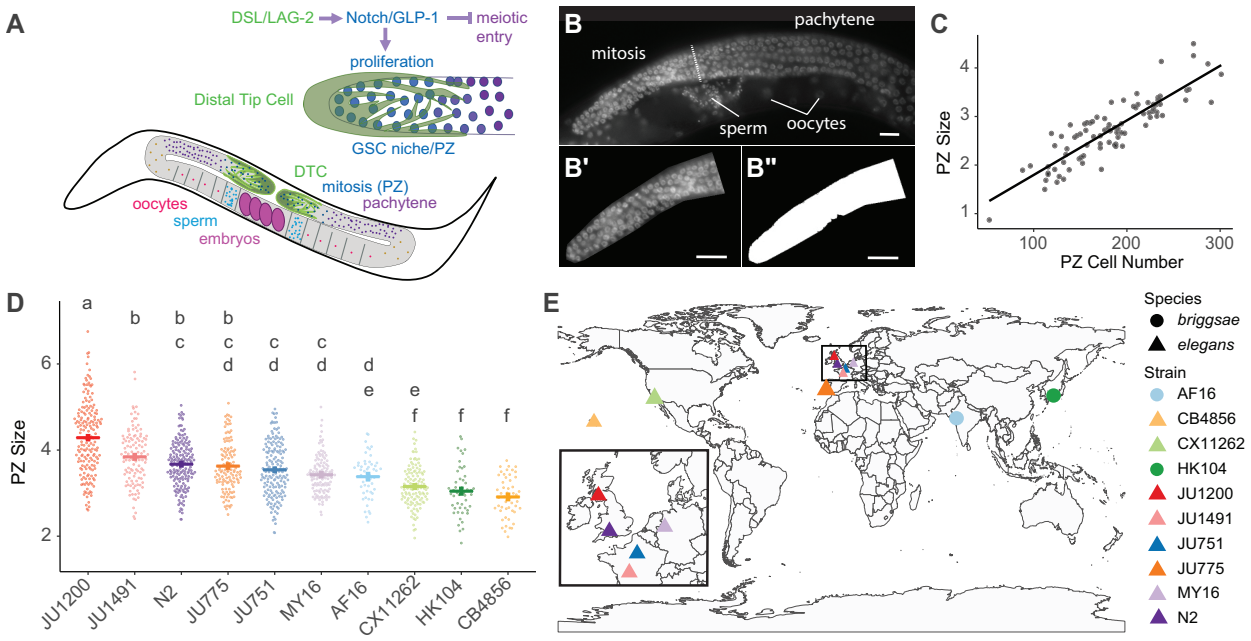

Figure 1. Germline progenitor zone size varies among natural *Caenorhabditis* populations.
A) The germline progenitor zone (PZ), also termed proliferative zone or mitotic region, located at the distal end of each gonad arm, contains mitotically dividing stem and progenitor cells. The germ stem cell (GSC) pool is maintained through Delta/Notch signaling by the somatic Distal Tip Cell (DTC), which enwraps distal PZ cells. The Delta/Serrate/LAG-2 (DSL-family) ligands, LAG-2 and APX-1, activate Notch (GLP-1) in germ cells to promote proliferation while also preventing meiotic entry. Germ cells differentiate into gamete progenitors through meiotic stages as they progress toward the proximal end of the arm. B) PZ size was used as a proxy for PZ cell number. Whole-mount worms were stained with DAPI and imaged under epifluorescence. The PZ boundary (dotted line) was identified as previously described based on the shape of germ cell nuclei (Crittenden and Kimble, 2008). B') The PZ region was manually cropped away from other tissues in ImageJ. B'') The PZ region was segmented from the background using a fluorescence threshold in ImageJ and the area of the PZ was calculated from the number of pixels. C) PZ area (scaled to PZ size based on pixel size, $\mu m^2/1000$) measured in this way correlates well with PZ cell number as counted by hand from z-stacks after DAPI staining (adj R^2 = 0.758, p<2.2e-16). D) PZ size ($\mu m^2/1000$) in young adult hermaphrodites (1-10 eggs *in utero*) of select wild isolates of *C. elegans* and *C. briggsae*. Lowercase letters indicate significant (p<0.05) Tukey-adjusted pairwise contrasts: isolates that share the same letters do not exhibit a significant difference in PZ size. E) World map showing the geographical origin of examined wild isolates. For statistical models and results see Tables S1-S2.

Germ cell proliferative activity differs between wild isolates JU1200 and JU751

Among the wild isolates that varied in PZ size, JU1200 (Scotland) and JU751 (France) exhibited significant and highly reproducible differences. JU1200 shows high genetic similarity with the laboratory strain N2[69]. As young adult hermaphrodites, JU1200 exhibited consistently more progenitor cells than JU751 (Figure 1D). We assayed PZ cell number in these two isolates from late larval to reproductive adult stages. While PZ cell number did not differ at the mid-L4 stage, JU751 showed significantly reduced PZ cell number relative to JU1200 across two stages of early adulthood (Figure 2A, Table S3).

Given that PZ size may not only be affected by proliferative activity but also by the transition rate towards the meiotic fate, we assayed mitotic activity using a 15-minute EdU (5-ethynyl-2-deoxyuridine) pulse to directly label and quantify proliferation rate in the PZ prior to the adult stage. At the mid-L4 stage, when PZ cell number in JU751 and JU1200 were not significantly different (Figure 2A), JU751 exhibited significantly reduced counts of EdU+ cells, and thus lower germ cell proliferative activity than JU1200 (Figure 2B, Table S4). Differences in germ cell proliferation thus contribute to the observed difference in PZ size between JU751 and JU1200.

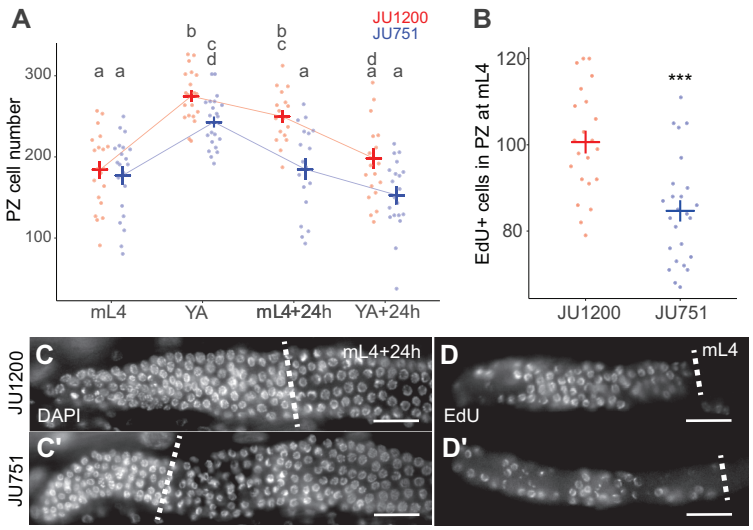

Figure 2. Germ cell proliferative activity differs between wild isolates JU1200 and JU751.
A) Number of PZ nuclei at mid-L4 larval stage (mL4), young adult (YA) with 1-10 eggs *in utero*, adult at 24 hours post-mid L4 (mL4+24h), and adult at 24 hours post-young adult (YA+24h). Nuclei were counted in z-stacks of extruded DAPI-stained gonads. Lowercase letters indicate significant ($p<0.05$) pairwise contrasts such that groups sharing the same letters are not significantly different. B) Number of EdU+ nuclei in the PZ after a 15-minute pulse of EdU at mL4 (*** $p < 0.001$). For statistical models and results, see Tables S3-S4. C) Representative images of the PZ in whole-mount DAPI-stained worms at mL4+24h. D) Representative images of EdU staining at the mid-L4 stage. Dotted lines mark the proximal boundary of the PZ. Scale bars are 20μm.

QTL mapping identifies multiple loci contributing to variation in PZ size

To characterize the genetic architecture underlying the observed differences in PZ size between JU751 and JU1200, we performed Quantitative Trait Locus (QTL) mapping based the phenotypes of F2 recombinant inbred lines (RILs) derived from these two isolates (Figures 3A and 3B)[70]. The RILs were constructed by selfing F1 hermaphrodites from reciprocal parental crosses and inbreeding the F2 lines for twelve generations to produce a panel of lines homozygous at each locus for one of the two parental genotypes (Figure 3B). We measured the PZ size of young adult hermaphrodites (1-10 eggs *in utero*) in 70 RILs and mapped the phenotypic differences to a genetic map derived from the recombination frequencies of 140 SNP markers throughout the genome (Figure 3A, Figure S1, Table S5). PZ size varied continuously across RILs and showed transgressive segregation, i.e. extreme phenotypes exceeding the parental phenotypes) (Figure 3A). We, therefore, employed a multi-QTL modeling approach using the R package, R/qtl[71]. As a first step, we performed a single QTL scan, an algorithm that calculates the likelihood that the genotype at any *single* locus can explain the phenotype data. This scan revealed a large-effect locus in the center of chromosome II with a 1.5-LOD interval of ~7.25 Mb (Figure 3C, green line). Next, we used a "two-QTL" algorithm to determine the likelihood that any *pair* of loci is associated with the phenotype. Importantly, this algorithm does not allow the loci to have opposing effects. The two-QTL scan revealed an additional locus on the left arm of chromosome V (~2.6 Mb) acting additively with the chromosome II (abbreviated QII) QTL (Figure 3D-F). Single-QTL mapping with the QII QTL as an additive covariate also revealed the chromosome V QTL (abbreviated QV) (Figure 3C, magenta line). An additional two-QTL scan, specifically allowing for interactions between loci with opposing effects, revealed two more potential QTL on chromosomes I (~1 Mb) and X (~2.7 Mb) (Figure 3G-I). We then performed multi-QTL model selection, using these four loci as candidates. We performed the model selection manually and also used a model-building

and pruning tool provided in R/qtl. This algorithm begins naïvely or with a specified model, adding loci through successive genome scans and assigning each model a penalized LOD score. It then prunes the model to achieve the simplest form with the highest penalized LOD score (LOD > 0 indicates that the model performs better than a model with zero QTL). A representative set of all the models tested, along with their penalized LOD scores, are shown in Figure 3J. We used both approaches and determined that our RIL data best support a model in which QII and QV act additively to determine PZ size. This model explained ~32% of the phenotypic variation in the RIL data (Table S6).

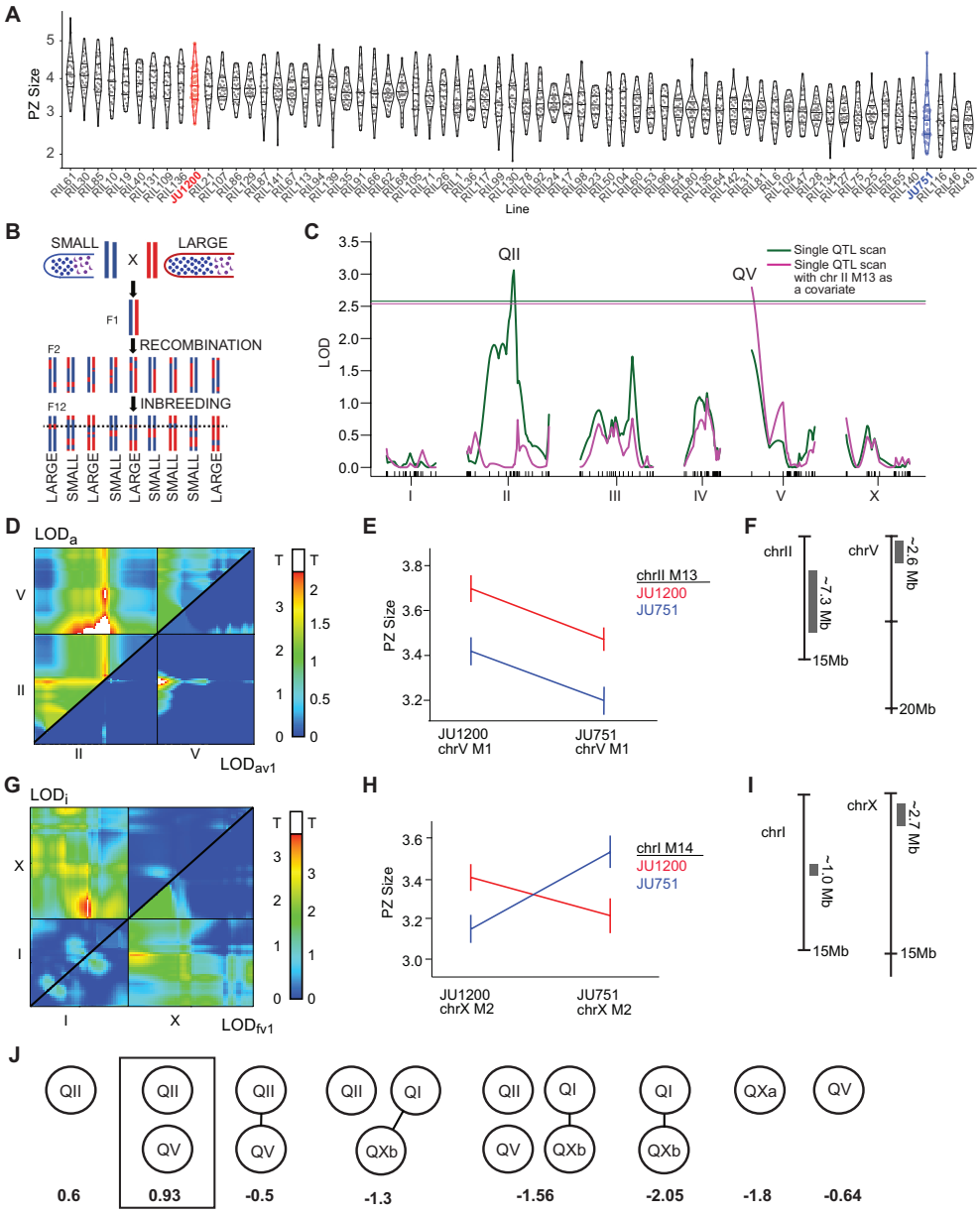

Figure 3. QTL mapping identifies multiple QTL explaining variation in PZ size
A) PZ size (μm^2/1000) measured in 70 F2 recombinant inbred lines (RILs) derived from a cross between wild isolates JU1200 (red) and JU751 (blue). B) Scheme illustrating the generation and analysis of the F2 RIL panel derived from the two parental isolates with different PZ size. The dotted black line indicates the location of a theoretical QTL. C) Results of single-QTL scans that interrogate each location on the genetic map for an association with the phenotype. The logarithm of odds (LOD) is shown on the y-axis and the horizontal lines indicates the significance threshold for each scan. The genetic map for each linkage group is shown on the X-axis. While the green line shows the results of a naïve scan, the magenta line shows the results of a scan in which SNP marker 13 at the center of QII (the peak in the magenta curve) is included as a covariate. In this scan, an additional QTL on chr V is detected. D) Results from a two-QTL scan that interrogates each pair of loci for a significant effect on the phenotype. The top half shows the LOD scores (LOD_a) comparing a strictly additive model for each pair of loci on chr II and V to the null model. The bottom half shows the LOD scores comparing the additive model with the single-QTL model for each pair of loci (LOD_{av1}). LOD_{av1} scores above threshold (white) indicate an improvement in fit over the single-QTL model. E) Interaction plot for a pair of markers that fall within the significant peak in the bottom half of panel D (chr V, marker 1 and chr II, marker 14). F) Approximate locations and sizes (based on 1.5 LOD intervals) of the QTL on chr II and V. G) Results from a two-QTL scan that interrogates each pair of loci for a significant effect on the phenotype, allowing for opposing effects. The top half shows the maximum LOD scores (LOD_i) comparing a full two-QTL model for each pair of loci on chr I and X to the additive model. The bottom half shows the LOD scores comparing the full model (allowing for interactions) with the single-QTL model for each pair of loci (LOD_{fv1}). LOD_i scores above threshold (white, as determined by permutation analysis) indicate evidence for an interaction between two loci, whereas LOD_{fv1} scores above the threshold indicate an improvement in fit over the single-QTL model. H) Interaction plot for a pair of markers that fall within the significant peak in the top half of panel G (chr I, marker 14 and chr X, marker 2). I) Approximate locations and sizes (based on 1.5 LOD intervals) of the candidate QTL on chr I and X. J) Graphic representation of multi-QTL model selection. Each node represents a candidate QTL (QII=chrII@35cM, QV=chr V@0cM, QI=chrI@23cM, QXa=chrX@16cM, QXb=chrX@2.5cM) and each spoke represents an interaction. Values below each model are the penalized LOD scores. Scores above zero indicate that the model performs better than the global null of zero QTL. For additional information on the mapping and statistical methods used, see materials and methods and Figure S1. For multi-QTL model statistics see Table S6. Analyses were carried out on raw data (PZ Area in pixels) and y-axes in (A), (E), and (H) were scaled to μm^2/1000 for presentation (0.1008 μm^2/pixel).

Validation of the chromosome II QTL through generation of near-isogenic lines (NILs)

To validate the effect of the chromosome II QTL (QII) on PZ size, we generated near-isogenic lines (NILs). Two RILs containing JU751 sequence in QII were backcrossed for 10 generations to JU1200 to produce two NILs containing JU1200 sequence in various segments of the QTL (Figure 4A). Two RILs containing JU1200 sequence in QII were backcrossed for 10 generations to JU751 to produce five NILs containing JU1200 sequence in various segments of the QTL (Figure 4B). NILs were generated by selecting for the presence of parent-specific PCR products in the QTL region. We assayed PZ size several times in each of the NILs. The NILs established in the JU1200 background showed subtle effects on PZ size, which were not always consistent across experimental assays (blocks) (Data S1). We, therefore, analyzed the aggregated results from across nine experiments using generalized linear models to account for experimental block effect and found that we could detect a small, but significant, reduction in PZ size (Figure 4C, Table S7). The NILs in the JU751 background showed larger and more consistent differences in PZ size, confirming the effect of QII on PZ size (Figure 4D, Table S8). Moreover, recombination events that had occurred during the backcrossing procedure allowed us to narrow down the QTL region from 7.25 Mb to 2.04 Mb (Figure 4B). Searching for JU751-JU1200 polymorphisms in this reduced genomic region uncovered a total of ~1024 variants (196 potential high-impact variants, i.e. variants predicted by a BCSQ algorithm to likely alter gene function, for example, through frameshift or nonsense mutations) in 250 distinct genes and 10 large INDELs (Data S1)[69]. However, we did not identify a strong candidate variant for further analysis.

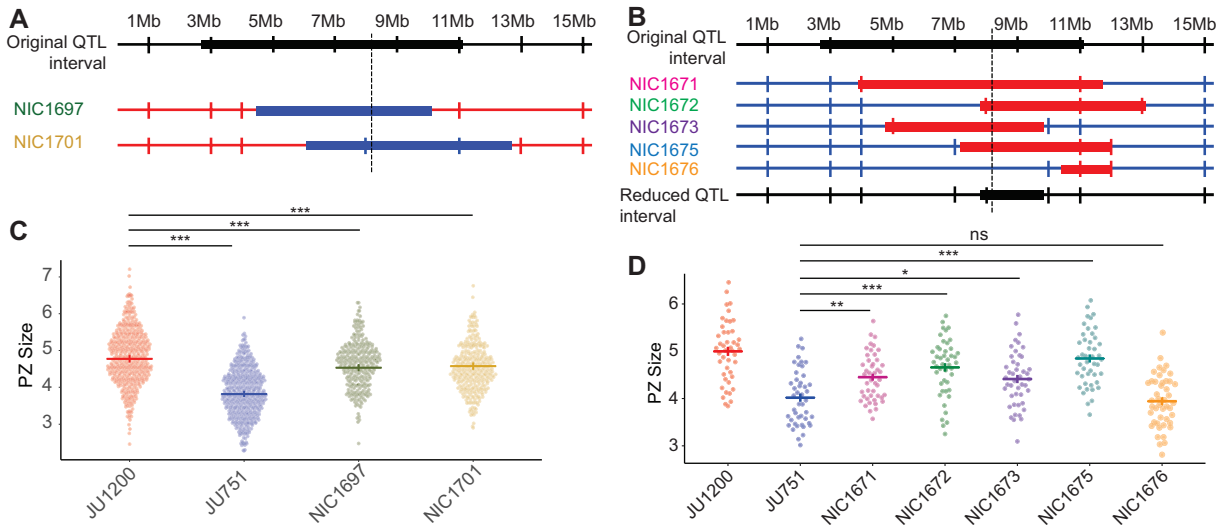

Figure 4. Validation of the chromosome II QTL through generation of near-isogenic lines (NILs)
A) Generation of NILs in the JU1200 background. Diagram showing the original QII QTL interval of ~7.25Mb on chr II, with the dashed vertical line indicating the approximate location of the LOD peak. Two RILs (RIL54/NIC654, RIL127/NIC727) containing JU751 sequence in QII were backcrossed for 10 generations to JU1200 to produce two NILs (NIC1697, NIC1701). Blue: JU751 genotype, red: JU1200 genotype. B) Generation of NILs in the JU751 background. Diagram showing the original QII interval of ~7.25Mb on chr II, with the dashed vertical line indicating the approximate location of the LOD peak of the original QTL. Two RILs (RIL128/NIC728, RIL71/NIC671) containing JU1200 sequence in QII were backcrossed for 10 generations to JU751 to produce five NILs (NIC1671, NIC1672, NIC1673, NIC1675, NIC1676. Blue: JU751 genotype, red: JU1200 genotype. C) PZ size measurements in NILs established in the JU1200 background shown in (A) and the parental isolates. D) PZ size measurements in NILs established in the JU751 background shown in (B) and the parental isolates. The reduced QII interval was determined by asking whether each NIL showed a significant increase in PZ size as compared to JU751. All NILs except NIC1676 had larger PZs than JU751. Therefore, the region over which the JU1200 segment in these NILs overlap was considered the reduced QTL interval (2.04 Mb). Analysis was carried out on raw data (PZ area in pixels), and the y-axes were scaled to $\mu m^2/1000$ for presentation (0.0504 μm^2/pixel). For statistical models and results see Tables S7 and S8 (* $0.01 < p \leq 0.05$, ** $0.05 < p \leq 0.01$, *** $p \leq 0.001$).

A 148 base pair deletion in the upstream regulatory region of the DSL ligand *lag-2* is a candidate causal variant in the chromosome V QTL

The 2.6 Mb region of QV contained only 21 presumptive candidate variants (SNPs, INDELS) contributing to PZ size differences between JU751 and JU1200 (Data S1). Inspecting these variants in detail revealed one major candidate: a deletion in JU751 upstream of the genomic region encoding the delta-like ligand, *lag-2*, a primary regulator of germ cell proliferation and differentiation in the Notch pathway[17,69]. We named this deletion *lag-2(cgb1007);* genotypes with this deletion are abbreviated from here forward as *lag-2p(-)*, whereas we refer to genotypes without this deletion as *lag-2p(+)*. This deletion spans 148 bp and is located in the *lag-2* promoter region, 2441 bp upstream of the transcription initiation site (Figures 5A and S2). The 3.3 kb upstream promotor region of *lag-2* contains six HLH-2 binding sites (E-boxes), which are necessary for robust *lag-2* transcription in the DTC[26,72]. The *lag-2(cgb1007)* deletion contains one of these conserved HLH-2 binding sites as well as most of a 30 bp poly(G) repeat (Figure 5A, S2, S3). This deletion could explain reduced germ cell proliferation observed in JU751 due to reduced *lag-2* transcription via the loss of a specific binding site for the transcription factor HLH-2[72].

Examining whole-genome sequence data of a global panel of over 1500 *C. elegans* wild isolates[69,73], we found the *lag-2(cgb1007)* deletion to be unique to the isolate JU751. A similar, but larger, deletion was found in two isolates from Asia, GXW1 and JU4073 (Figure S3C and S3D). Since no other isolates were found to carry the *lag-2(cgb1007)* deletion, we wondered if this deletion could have arisen after isolation, during laboratory culture. We, therefore, examined

additional isolates (for which no whole-genome sequence data exist) that were collected from the same habitat (compost) and location (Le Perreux-sur-Marne, France) as JU751 in 2004 and 2005[74]. All other isolates (N=5) that were collected together with JU751 from this locality on the same day shared a highly similar haplotype and also carried the *lag-2(cgb1007)* deletion. In contrast, all examined isolates with different haplotypes, collected at other dates throughout 2004 and 2005 (N=13) did not carry the deletion[70] (Figure S3). We conclude that the *lag-2(cgb1007)* deletion was acquired before isolation in the laboratory and that this allele is likely rare in natural populations.

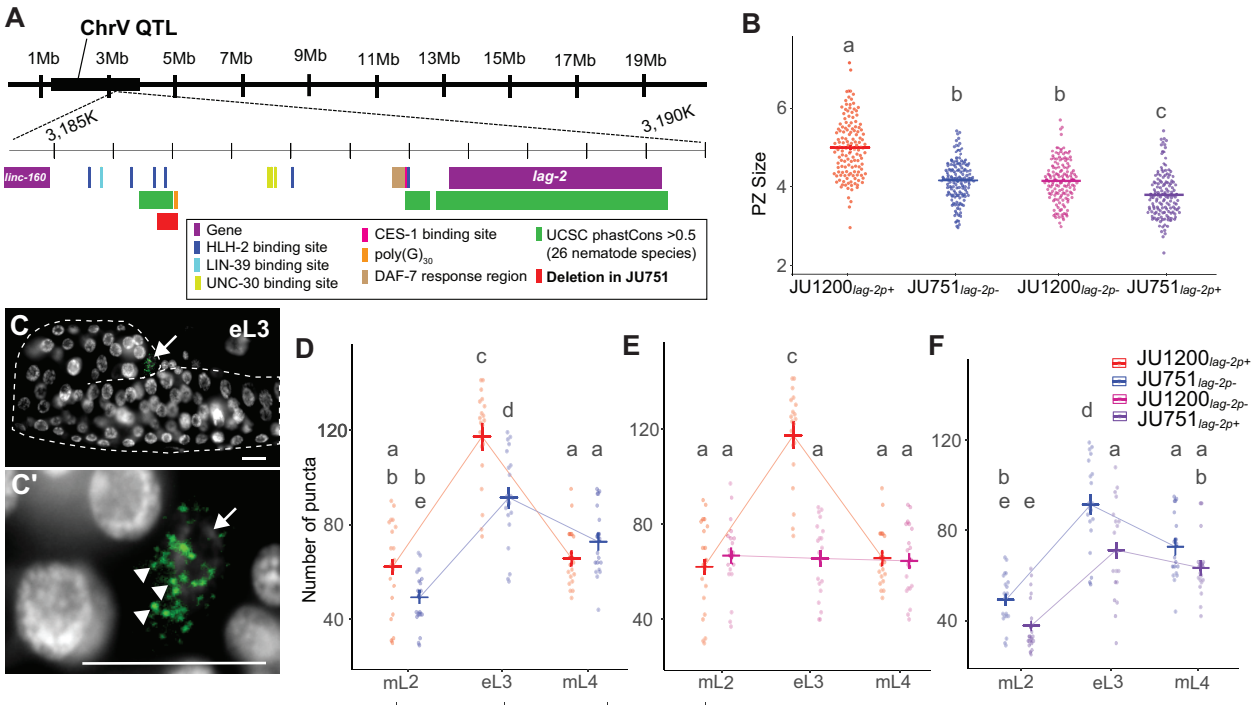

Figure 5. A 148 base pair deletion in the upstream regulatory region of the DSL ligand *lag-2* has background and stage-specific effects on *lag-2* expression and PZ size.
A) Diagram of the QV QTL (black bar) and a 5 kb region within it containing the *lag-2* gene and its 3 kb upstream sequence. The well-characterized *lag-2* promoter contains several known transcription factor binding sites including six HLH-2 E-boxes (dark blue) (Chesney et al., 2009; Karp and Greenwald, 2003). JU751 has a 148 bp deletion (red) overlapping the third HLH-2 binding site and most of a 30 bp polyG repeat (orange). The locations of all promoter elements and UCSC phastCons statistics (green) were taken from the wormbase.org (version WS283) JBrowse tool. B) The size of the PZ ($\mu m^2/1000$) in the parents and allelic replacement lines (ARLs) at the young adult stage. C) Representative images used for smFISH quantification of *lag-2* transcripts in the DTC at mid L3 (*lag-2* mRNA green, DAPI [DNA] white, scale bar 10μm). C) The gonad arm is outlined by a dashed line. The arrow marks the DTC. C') Higher magnification of C. Arrow indicates the DTC. Arrowheads indicate individual puncta, which were quantified to determine *lag-2* expression levels. D-F) Quantification of *lag-2* mRNA puncta via smFISH. Crossbars and error bars represent estimated marginal means +/- standard error from a single generalized linear model. Data from a single experiment were split into three graphs for clarity. Groups with different lowercase letters are significantly different ($p<0.05$) according to Tukey-adjusted pairwise contrasts. Analysis was carried out on raw data (PZ area in pixels), and the y-axes were scaled to $\mu m^2/1000$ for presentation (0.0504 μm^2/pixel). For statistical models and results see Tables S9-S10.

Restoring the genomic region of the *lag-2(cgb1007)* deletion does not increase but reduces PZ size in JU751

To validate that the *lag-2(cgb1007)* deletion genomic region contributes to differences in germline PZ size between JU751 and JU1200, we created reciprocal allelic replacement lines (ARLs) using CRISPR-*Cas9* genome editing. First, we introduced the deletion into JU1200, resulting in the strain JU1200$_{lag\text{-}2p(-)}$. Second, we restored the deleted *lag-2* promoter region in JU751, resulting in the strain JU751$_{lag\text{-}2p(+)}$. As predicted, removing the 148 bp fragment in the JU1200 background strongly reduced PZ size (Figure 5B). In contrast, and contrary to expectations, restoring the corresponding fragment in the JU751 background did not increase but further reduced PZ size (Figure 5B and Table S9). Although the *lag-2(cgb1007)* deletion is sufficient to decrease PZ size to a similar extent as in JU751 when introduced in the JU1200 background, it cannot be the only genetic variant contributing to the difference of PZ size observed between JU751 and JU1200. In other words, the effects of the *lag-2(cgb1007)* deletion are strongly dependent on the genetic background. This is in line with our QTL analysis, in which the marginal effect of the QV QTL was only detectable when accounting for variation at the QII QTL (Figure 3C). Furthermore, while *lag-2(cgb1007)* has clear effects on PZ size, and therefore contributes to the overall effect of QV, we cannot rule out other causal variants within the QV QTL region.

Differences in *lag-2* expression recapitulate genotypic differences in PZ size

Given the result above, we next wanted to directly determine whether and how observed genotypic differences in PZ size can be explained by differences in *lag-2* expression. Using single molecule fluorescence *in situ* hybridization (smFISH)[75,76], we quantified *lag-2* transcripts in the DTCs of the parental isolates and reciprocal ARLs, JU1200$_{lag\text{-}2p(-)}$ and JU751$_{lag\text{-}2p(+)}$. We first measured *lag-2* expression in parental isolates and found that expression was considerably higher during larval development than in the adult stage, with strongest expression during the early L3 stage (Figure S4 and Table S12). Quantifying *lag-2* expression in parental isolates and reciprocal ARLs across three larval stages, we found that at the early L3 stage (but not at mid-L2 or at mid-L4), JU1200 showed significantly higher *lag-2* expression relative to JU751 (Figure 5D and Table S10), consistent with its larger PZ size. Remarkably, relatively higher expression of *lag-2* in JU1200 at the L3 stage was completely abolished in JU1200$_{lag\text{-}2p(-)}$, which showed very similar expression levels as JU751 across all three developmental stages (Figure 5E, Table S10). These results are consistent with past results showing that the *lag-2* promotor E-boxes are required for robust *lag-2*::GFP transgene expression during the L3 stage[72]. Inserting the 148 bp *lag-2* promoter sequence into the JU751 background did not result in higher *lag-2* expression at L3 relative to JU751. Instead, *lag-2* expression in JU751$_{lag\text{-}2p(+)}$ was lower at L3 with similar trends in expression changes among the stages (Figure 5F, Table S10). This result confirmed that the unexpected reduction in PZ size of JU751$_{lag\text{-}2p(+)}$ is indeed causally linked to reduced *lag-2* expression. Overall, these smFISH measurements show that *lag-2* expression (at the L3 stage) tightly recapitulates observed phenotypic differences in PZ size at the early adult stage and confirm that the effects of the *lag-2(cgb1007)* deletion are strongly dependent on the genetic background. Analysis of the parental isolates also shows that natural differences in *C. elegans* germ stem cell niche activity can be directly linked to differences in the expression of a core signaling component, the Notch ligand *lag-2.*

Higher-order epistatic interactions shape natural variation in PZ size

Given the apparent epistatic interactions between the *lag-2* promoter variant and the genetic backgrounds, we built a more exhaustive model to account for additional two- and three-way interactions among 1) central portions of the chromosome II QTL isolated in our NILs (abbreviated "C2" to distinguish it from the full QII QTL—with genotypes *C2-JU1200* or *C2-JU751*), 2) the *lag-2* promoter variant (abbreviated "C5"—with genotypes *lag-2p(+)* or *lag-2p(-))*, and 3) the genetic background ("BGND"—JU1200 or JU751). To do this, we generated a large data set containing

all eight possible genotype combinations (labeled i to viii) (Figure 6A). Analyzing this data set revealed both subtle and dramatic two- and three-way interactions (Figure 6B to 6E). To explore these data in detail, we built a generalized linear model, using a "top-down" model selection strategy to optimize the Bayesian information criterion (BIC) and the adjusted deviance accounted for in the model (D^2)[77] (Table S11). The optimized model indicated that PZ size is best explained by all three main effects and all of their interactions (i.e., fully-crossed). In addition, the model includes a fixed main block effect and interactions to account for variation across different experimental blocks. The model accounts for 33.4% of the adjusted deviance and fits the data well (χ^2 =2796.5 on 2763 df; p = 0.324) (Table S11).

To interpret the model, it is helpful to compare the estimated marginal means (Figure 6B, Table S11B). Examining the genetic interactions of the two loci and genetic background reveals widespread and strong epistasis explaining variation in PZ size. As mentioned earlier (Figure 5B), the *lag-2(cgb1007)* deletion has opposing phenotypic effects depending on the genetic background: the deletion strongly reduces PZ size in JU1200 but increases PZ size in JU751 (Figure 6B). Examining the epistatic interactions shows that the effects of the *lag-2(cgb1007)* variant are highly contingent on both C2 and genetic background, so that the *lag-2* deletion may have negative, positive or no phenotypic consequences across the set of genotypes (Figures 6B-E). Similarly, the phenotypic effects of C2 are strongly dependent on the genetic context: *C2-JU751* reduces PZ size in every genotype (Figure 6B—i vs. ii, v vs. vii, and vi vs. viii) *except* $JU1200_{C5\text{-}lag\text{-}2p(-)}$ (Figure 6B—iii vs. iv). The presence of the *lag-2* deletion dampens the effect of *C2-JU751* in the JU1200 background (Figure 6E' and 6E''), which could imply that alleles within C2 act, at least in part, through this region of the *lag-2* promoter. As one might expect, the combined effect of all other unidentified variants in the genetic background has the greatest influence on PZ size overall. Yet, this effect does vary remarkably depending on the presence of *lag-2p* deletion and genotypes at C2. In general, the JU751 background strongly reduces PZ size (Figure 6C', 6C''), but there is no significant difference between $JU1200_{C2\text{-}JU1200}$ and $JU751_{C2\text{-}JU1200}$ when the *lag-2* deletion is present (Figure 6B—iv vs. v, and 6C'). We interpret this to mean that, in presence of the *lag-2* deletion (*lag-2p(-)*), *C2-JU1200* variants exert a strong positive effect to maintain PZ size despite the average negative effect of variants in the JU751 background (Figure 6D'', red line). Conversely, *C2-JU751* variants cannot maintain this positive effect resulting in background sensitivity (Figure 6D'', blue line). Finally, without the *lag-2p* deletion (*lag-2p(+)*), the *C2-JU751* variants do not modify the strong negative effect of the JU751 background (Figure 6D' vs 6D'' red lines).

Our model shows that higher-order epistatic interactions contribute to variation in *C. elegans* PZ size. Importantly, some of the observed phenotypic effects are masked when only two-way interactions are considered (for example, Figure 6E vs. E' and E''). These results highlight the need for caution when interpreting the phenotypic effect of a variant or allele, as the effect may be highly contingent on other variants in the genetic background. We also stress that even our interpretations of the effects of C2 and the genetic background must be considered with care as they are aggregate effects, which may be influenced by underlying epistatic interactions and, possibly, additive effects of closely linked loci.

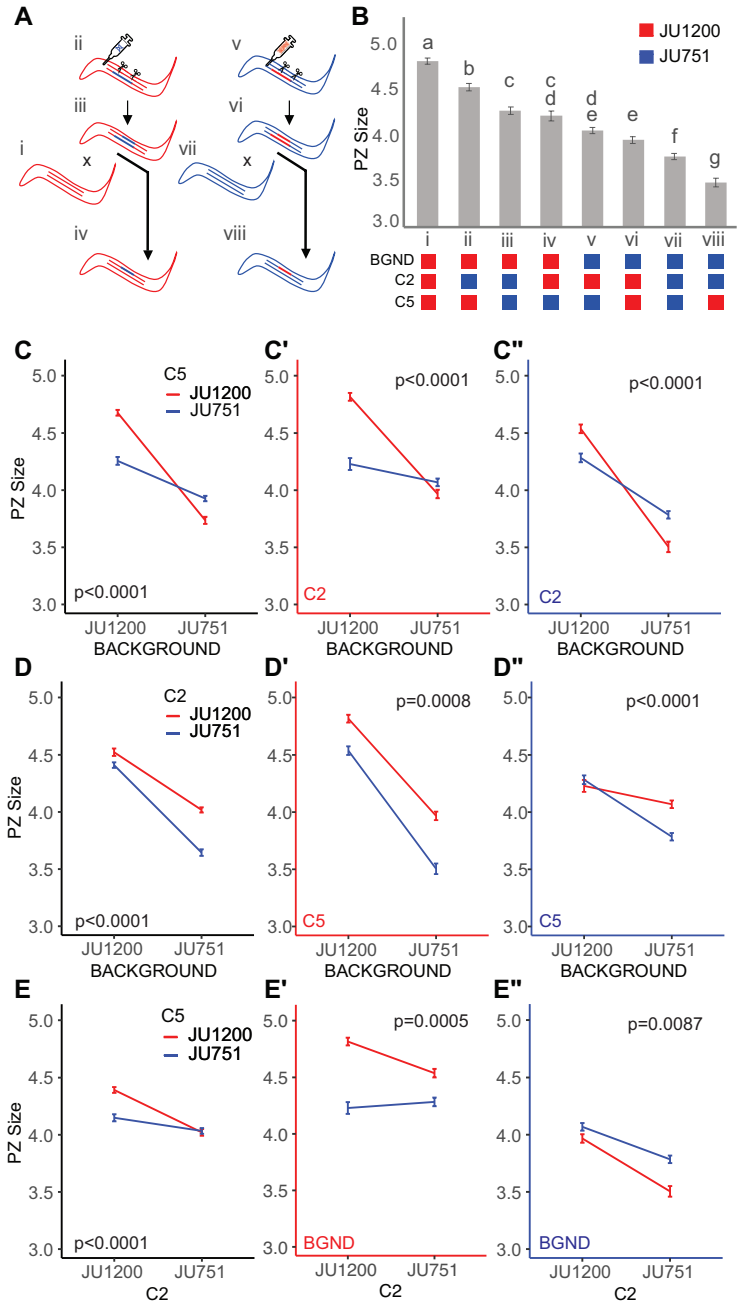

Figure 6. Higher-order epistatic interactions shape natural variation in PZ size
A) Scheme depicting the generation of the eight genotypes used in the interactions analysis. The different genotypes were derived by made either creating or replacing the *lag-2(cgb1007)* deletion in JU1200 and JU751 background NILs. The successfully modified lines were then backcrossed to the parental lines to isolate the CRISPR modifications in the parental backgrounds. Genotypes are labeled i-viii for clarity. B) Estimated marginal means +/- SE of PZ size from a generalized linear model describing a data set containing all eight genotypes. JU1200 and JU751 genotypes are indicated by red and blue, respectively, and are indicated for each of the loci and background below the chart. Lowercase letters indicate significant (p<0.05) Tukey-adjusted pairwise contrasts such that groups that share a letter are not significantly different. C-E) The same model data as in (B) presented to show interactions among the loci and background. Graphs with black axes show only two-way interactions. The third dimension is represented as a split into two graphs with red and blue axes indicating the genotypes for the locus given in the bottom left. Two-way interaction p-values are given in the graphs. Analysis was carried out on raw data (PZ area in pixels), but the y-axes were scaled to μm^2 for presentation (0.0504 μm^2/pixel) (see Table S11 for model details).

DISCUSSION

Our study explores the natural variation and quantitative genetic architecture of a germ stem cell system. Examining only a handful of *C. elegans* wild isolates, we were able to detect significant differences in germline progenitor zone (PZ) size, indicative of variation in germ stem cell niche activity. Our main findings are: (1) Natural variation in PZ between two isolates maps to multiple, partly interacting QTL. (2) Resolving a QTL on chromosome V identified a deletion in the promoter region of the DSL ligand *lag-2*, a known key signal promoting the germ stem cell fate via the Notch pathway. (3) Natural quantitative variation in *C. elegans* germline proliferative activity arises through modulation of transcriptional activity of core signaling elements of the germ stem cell niche. (4) Using introgression and allelic replacement lines, we show that main effects and interactions of the two QTL on chromosomes II and V (*lag-2* deletion) are partly antagonistic and highly contingent on the genetic background. (5) Hence, higher-order epistatic interactions shape natural variation in germ stem cell niche activity.

Germ stem cell niche activity is a complex trait

Our observations suggest that *C. elegans* germ stem cell niche activity is a typical complex trait involving a polygenic architecture. Additional observations support this view indirectly: (1) PZ size varies continuously, and often subtly, in natural populations (this study); (2) the *lag-2* deletion was not found in other wild isolates with small PZ size (this study); and (3) mutations in large number of genes modulate PZ size and these genes exhibit diverse functions that not only act in germ stem cell proliferation, cell cycle progression and differentiation, but also in diverse metabolic or sensory processes[17]. Together with our findings, these observations suggest that *C. elegans* PZ size is a higher-order phenotype that likely integrates effects of allelic variation at many loci. In the case of our example, focusing on two target isolates with pronounced differences in PZ size, we also identified large-effect loci or variants on chromosomes II and V whose effects were partly antagonistic and, overall, strongly dependent on the genetic context. Together, and in line with previous studies, this suggests that the effects of large-effects variants, even if resolved at the molecular level (such as the *lag-2(cgb1007)* deletion), can be misleading if epistatic interactions in the native background are ignored[4,78].

Epistatic interactions underlie additive genetic variance

Performing QTL mapping on a panel of F2 RILs, derived from two parental isolates with divergent PZ size, we detected four, partly interacting QTL. In the best model identified by our multi-QTL model selection approach, the QII and QV QTL act additively to explain 32% of the phenotypic variance in the examined RIL population. However, analysis of introgression and allelic replacement lines uncovered extensive epistatic interactions among these loci and the genetic background. This finding is not surprising given that gene-gene interactions contribute to the component of additive genetic variance (V_A) measured at the population level; that is, high V_A variance need not reflect additive gene action[7,79–86]. In particular, measures of V_A due to individual loci will strongly depend on allele frequencies of all loci that are epistatic to each other. Hence, measures of V_A (and other genetic variance components, including the epistatic variance) provide little to no information about underlying epistatic interactions, and hence, genetic trait architecture, even when QTLs have been detected. Characterizing the molecular nature of QTLs and their interaction in controlled genetic backgrounds is, therefore, essential.

Natural variation in *lag-2* expression

Resolving the QV QTL region identified a unique 148 bp deletion in the *lag-2* promoter region of JU751, *lag-2(cgb1007).* This deletion removes one of six E-box sites required for binding of HLH-2, a positive regulator of *lag-2* mediated germ cell proliferation and germline expansion[26,72]. Mutating these E-box sites was shown to result in reduced *lag-2::GFP* transgene expression specifically during the L3 stage (and subsequently reduced germ cell proliferation)[72]. We,

therefore, expected *lag-2(cgb1007)* to cause reduced *lag-2* expression due to reduced HLH-2 binding activity. Consistent with this scenario, introducing this deletion into JU1200 (with a large PZ size) significantly reduced both PZ size and *lag-2* expression in the DTC (Figure 5B and 5E). In contrast, restoring the corresponding ancestral sequence (JU1200) of this deletion in JU751 (with a small PZ size) further reduced, rather than increasing, PZ size along with *lag-2* expression (Figure 5B and 5F). The *lag-2* deletion allele on its own, therefore, exerts opposing effects depending on the genetic background (sign epistasis). However, examining the interaction between the *lag-2(cgb1007)* deletion (C5) and a central portion of the chromosome II QTL (C2) shows that *C2-JU1200* can dampen this reversal (Figure 6C' vs. C"). In addition, the *lag-2* deletion modifies the effect of C2 by dampening the negative effects of *C2-JU751* in both backgrounds (Figure 6E' vs. E"). This indicates that C2 interacts with the *lag-2* promoter region, specifically in the region of the *lag-2(cgb1007)* deletion. We do not have any hypotheses regarding the molecular nature of this interaction as none of the genes (*hlh-2, lin-39, unc-130, daf-3/daf-5, ces-1*) with confirmed binding sites or response elements in the *lag-2* promoter region are located within the C2 region. Moreover, although coding polymorphisms (JU1200 versus JU751) exist in some of these genes (*lin-39*, *unc-130*, and *daf-5*) none occur in *hlh-2*, *daf-3* and *ces-1*[69]. Resolving the QII QTL would, therefore, be required to dissect this genetic interaction. Overall, the *lag-2* deletion containing an HLH-2 binding site previously shown to positively effect *lag-2* expression in N2, can have positive, negative, or neutral effects depending on the genetic context (Figure 6).

Although it remains unclear whether and how the *lag-2(cgb1007)* deletion contributes to reduced PZ size in JU751, our smFISH measurements of *lag-2* transcripts in the DTC provide unambiguous support that differences in *lag-2* transcriptional activity contribute to observed differences in germ stem cell niche activity observed between JU751 and JU1200. *lag-2* smFISH measurements closely mirrored PZ size measurements not only in parental isolates but also in reciprocal ARLs, in which the *lag-2* promoter fragment was manipulated (Figure 5B). Identification and characterization of this variant shows that natural variation in PZ size can occur through direct modification of core signals of the *C. elegans* stem cell niche. However, we cannot rule out additional contributions from other unidentified variants in the QV QTL.

Fitness relevance of PZ size and its natural variation

While activity of any germ stem cell system is obviously relevant for organismal reproductive fitness, it is not clear whether and how observed natural variation in germ cell proliferation (and PZ size) might translate into variation in reproductive fitness. Although increased germ cell proliferation has been found to correlate with increased egg-laying activity, offspring production, and egg quality[10,17,28,30,57,87,88], it is unclear to what degree this relationship is causal: *C. elegans* primarily reproduces through self-fertilizing hermaphrodites, which sequentially produce sperm, then oocytes for the remainder of life. In laboratory conditions, this causes *C. elegans* fecundity to be limited by the amount of self-sperm (~250) initially produced. PZ size is generally measured, as in our study, during the early adult stage, so that likely many of the observed progenitor cells will never develop into mature oocytes and become fertilized under selfing. However, increased germ cell proliferation allows for improved oocyte quality by upregulating the flux and number of oocytes undergoing physiological cell death (apoptosis), hence liberating resources to upregulate provisioning of surviving oocytes[10,17,28,30,57,87,88]. Therefore, while adult PZ size need not reflect a direct proxy for future reproductive potential of selfing hermaphrodites (offspring number), it potentially increases resource provisioning of oocytes, thereby enhancing offspring quality. In addition, adult PZ size also reflects past proliferative activity of earlier larval stages, as illustrated by our quantifications of proliferative activity (Figures 2B and 5D). Variation in adult PZ size may thus reflect differential reproductive investment during larval development, which may trade-off with energy allocation to somatic development.

With regard to reproductive fitness differences of the target isolates in our study, JU751 and JU1200, we have previously shown that selfing JU751 hermaphrodites have significantly

reduced brood size relative to JU1200[70]. This reduction is not caused by differential sperm production but partly due to a major-effect variant causing early matricidal hatching in JU751[70]. Still, even after correcting for this genetic variant in JU751, brood size remains significantly smaller in JU751 relative to JU1200[70]. Possibly, reduced germ cell proliferation (and smaller adult PZ) in JU751 could thus reflect a lower reproductive investment. Of course, this scenario is highly speculative and observed differences need not be adaptive. Similarly, we ignore whether any of the detected QTL, including the *lag-2(cgb1007)* deletion, are maintained by selection. Even if selectively advantageous, the QTL variants could have been selected because of their effects on germline proliferative activity or unknown pleiotropic effects.

Limitations of QTL mapping and interpretation of epistatic interactions

Here we focused on the analysis of two large-effect QTLs and their interactions, detected using a rather small panel of RILs (N=70). Therefore, detecting small-effect and additional epistatic interactions through QTL mapping were unfeasible given the relatively low statistical power. Nevertheless, a specific search for interacting loci with opposing effects yielded two candidate QTL on chromosomes I and X (Figure 3H). Further analysis of this antagonistic interaction will likely be limited by its relatively small effect size and the already complex interactions between the chromosome II QTL, *lag-2(cgb1007)*, and the genetic background. In addition, further fine-mapping experiments are required to fully understand epistatic interactions between the QII and QV QTL uncovered here. Both QTL could harbor multiple loci affecting PZ size variation, potentially also including closely linked, antagonistically loci, which seem to be common in *C. elegans*[78].

Beyond these technical limitations, a number of other issues complicate the interpretation of our findings. First, and foremost, artificial mapping populations, such as the F2 RIL panel used here, may generate novel epistatic interactions through disruption of linked genomic regions. This is particularly relevant for the predominantly selfing *C. elegans*, with low effective recombination leading to strong linkage disequilibrium[73,89–91]. Most prominently, crosses between wild isolates of selfing *Caenorhabditis* have uncovered consistent, strong outbreeding depression due to widespread genetic incompatibilities reducing survival and reproduction[90,92–95]. Such epistatic interactions of novel allelic combinations generated in artificial *C. elegans* populations are thus particularly likely to affect traits that involve a polygenic architecture[4,78,96–98]. In other words, epistatic interactions observed in artificial mapping panels need not necessarily reflect epistatic interactions that occur in the wild. Nevertheless, their study does provide insight into the genetic architecture underlying trait variation.

Conclusions

Together with past research, our study reinforces the view that generalizations on trait architecture based on the isolated study of individual molecular variants in single genetic backgrounds are likely misleading. Combining quantitative and developmental genetic approaches is, therefore, essential to understanding complex quantitative trait architecture in the face of epistatic and often idiosyncratic interactions. Given that currently (and likely for a long time) even the most sophisticated experiments can interrogate only a tiny fraction of all possible epistatic interactions, integrating developmental and quantitative genetic approaches affords the best option to bring us one step closer to understanding the genetic basis of phenotypes and their variation.

ACKNOWLEDGEMENTS
We would like to thank Nausicaa Poullet, Anne Vielle, and Clotilde Gimond for contributions to experimental work that initiated this project. We thank Fabien Duveau, Marie-Anne Félix, Luke Noble, Clotilde Gimond, Laure Mignerot and Joao Picao Osorio for discussion, helpful comments on previous versions of the manuscript, and technical advice. *C. elegans* strains were kindly provided by the *Caenorhabditis elegans* Natural Diversity Resource (*Ce*NDR) and Marie-Anne Félix. CB acknowledges funding by the Fondation ARC sur la recherche sur le cancer (PJA 20161205047). SRF was supported by a post-doctoral fellowship from the City of Nice, France (Ville de Nice: Aides Individuelles Jeunes Chercheurs). We acknowledge additional financial support by the Centre National de la Recherche Scientifique (CNRS), the Institut national de la santé et de la recherche médicale (Inserm), and the Université Côte d'Azur (UCA).

AUTHOR CONTRIBUTIONS
Conceptualization, S.R.F and C.B; Methodology, S.R.F, A.S. C.B.; Investigation, S.R.F., B.B., and A.S.; Formal Analysis and Visualization, S.R.F.; Writing—Original Draft, S.R.F.; Writing—Review and Editing, S.R.F., C.B.; Supervision and Project Administration, C.B.; Funding Acquisition, C.B., S.R.F.

DECLARATION OF INTERESTS
The authors declare no competing interests.

MATERIALS and METHODS

Experimental model
All *C. elegans* strains used in this study are listed in the Key Resources Table. Standard *C. elegans* methods[99–101] were used to maintain all strains (2.5% agar NGM plates seeded with *E. coli* strain OP50).

Method details
Quantification germline progenitor zone nuclei
Images of dissected gonads fixed in 100% ice cold methanol and stained with DAPI (VECTASHIELD® Antifade Mounting Medium with DAPI) were taken using an Olympus BX61 microscope (RRID:SCR_020343) with a CoolSnap HQ2 camera. Z-stacks with 1µm increments were performed in the DAPI channel at a 40x magnification. The nuclei were counted by hand using ImageJ (RRID:SCR_003070). First, the PZ was defined as the region adjacent to the distal tip cell ending at the transition zone boundary where two or more crescent shape nuclei per row of germ cells can be observed[37]. The stack of images was cropped at the progenitor zone to transition zone boundary and nuclei were counted.

Quantification of germ cell mitosis
Mitotic germ cell proliferation was quantified in L4 larvae using the Click-IT EdU kit from Thermofisher (Cat: C10338) according to the manufacturer's instructions unless otherwise noted. Briefly, worms were synchronized via hypochlorite treatment (1:1:2 Bleach:1M NaOH:ddH2O for 6 min then spin and wash 3x in M9) and eggs were allowed to hatch overnight in M9 at 20°C. Eggs were plated at a density of ~400 eggs/plate and allowed to develop until L4. Mid-L4 larvae (and later young adults with 1-10 eggs *in utero*) were isolated, washed, and allowed to soak in 100uL of 20mM EdU in M9 buffer for exactly 15 minutes (sufficient time to stain 50-75% of the PZ in young adults). Worms were quickly washed in M9 to remove EdU, and the gonads were

released by cutting on adherent glass slides (Fisherbrand™ Superfrost™ Plus Microscope Slides). A small amount of levamisole was used to anesthetize the worms. Dissected gonads were carefully washed on the slides, fixed in 4% PFA, and washed again. Washes were performed by application of small volumes of solution directly to the tissue on the slides followed by careful aspiration. After a final wash in dH2O, tissue was dried on a slide warmer (35°C for 5 min) to adhere tissue to slides. Slides were soaked in 100% MeOH at -20°C overnight. The following day, tissues were rehydrated in PBST and EdU staining was performed using the Click-IT EdU kit according to the manufacturer's instructions. The Click-IT staining protocol was repeated once and then slides were mounted with VECTASHIELD® Antifade Mounting Medium with DAPI. Imaging was performed through a 40x objective on an Olympus BX61 microscope (RRID:SCR_020343) with a CoolSnap HQ2 camera. Z-stacks were taken though the distal gonad (one per worm). EdU-positive and DAPI-stained PZ nuclei were counted by hand.

Estimation of PZ size

Quantifying PZ germ cell number can be a rate-limiting step in the scoring of PZ size among many samples. To overcome this obstacle, we developed a simple method of estimating PZ size and used this as a proxy for PZ cell number (Figure 1B and 1C). In brief, lines were synchronized by hypochlorite treatment (1:1:2 Bleach:1M NaOH:ddH2O for 6 min then spun and washed 3x in M9). Eggs were allowed to hatch in M9 buffer at 20°C overnight. The following day, the eggs were plated at a density of ~400 worms/plate on standard NGM media seeded with OP50. Larvae were allowed to develop into young adults at 20°C. Young adults were collected by washing the plates when the majority of animals showed 1-10 eggs *in utero*. Samples were washed in M9 and fixed in ice-cold methanol for at least 5 min. To prepare samples for imaging, worms were rehydrated in M9 and applied to glass slides with Vectashield mounting medium containing DAPI (Vector Laboratories, Burlingame, CA). The distal germlines of young adult hermaphrodites (containing 1-10 embryos *in utero*) were imaged through a 40x objective on an Olympus BX61 microscope (RRID:SCR_020343) with a CoolSnap HQ2 camera. One gonad arm was imaged per worm, that being the arm which happened to be closer to the objective lens. A single image was taken for each worm, with the plane of section capturing most of the nuclei on one side of the gonad such that crescent-shaped nuclei were visible, and the shape of the gonad in that plane was representative of any plane (Figure 1B). PZ size was then quantified for each image. The progenitor zone was defined as the region adjacent to the distal tip cell ending at the transition zone boundary where two or more crescent-shaped nuclei per row of germ cells can be observed[37]. The PZ was cropped away from all other tissues using ImageJ, and the threshold tool was used to maximize the number of PZ nuclei highlighted while minimizing highlighted background. The number of pixels highlighted was recorded as "PZ Area". This method of estimation correlates well with hand counts of PZ nuclei (Figure 1C).

RIL phenotyping and QTL mapping

We quantified PZ size in a set of 70 SNP-genotyped RILs derived from the two parents, JU1200 and JU751[70,102]. Lines were divided into six scoring blocks and scored over the course of eight weeks. PZ size was normalized across blocks using a correction factor. The correction factor was derived from the least square means of each block (lsmeans package v. 2.30-0) to each observation (correction factor = $LSM_{BlockX}/LSM_{Block1}$). Normalized PZ size was mapped using the software package R/qtl (v. 1.50)[71]. First, a genetic linkage map was derived from the SNP genotypes of all 70 RILs. Then, single QTL and two-QTL standard interval mapping based on hidden Markov models was used to identify candidate QTL. LOD thresholds were set to the 95th percentile of the maximum genome-wide LOD scores derived from 5000 random permutations of the data under the global null hypothesis of zero QTL. These candidate QTL served as the starting point for multi-QTL modeling in which the R/qtl software generates "penalized LOD scores" for each tested model. Models that perform better than the null hypothesis of zero QTL have

penalized LOD>0. We selected the model with the highest penalized LOD score as recommended by the authors of R/qtl[71] (Figure 3J).

NIL generation and chr II QTL genotyping

To validate the genomic interval of the QTL on chromosome II, we constructed nearly isogenic lines (NILs). Two RILs with JU1200 sequence in the QTL region (RIL128/NIC728 and RIL71/NIC671) and two RILs with JU751 sequence in the QTL region (RIL127/NIC727 and RIL54/NIC654) were backcrossed for 10-12 generations to isolate the region in the opposite parent's background. Lines were selected at each generation based on PCR genotyping of several INDELS in the chromosome II QTL (See Table S13 for primers and Table S14 for lines created and their genotypes).

Generation of allelic replacement lines (ARLs) and CRISPR/Cas-9 gene editing

In order to validate the candidate INDEL upstream of *lag-2* in the chromosome V QTL, we created reciprocal allelic replacement lines (ARLs) using CRISPR/Cas-9 editing using a protocol similar to that described by[103]. To introduce the deletion (*cgb1007*) into the JU1200 background, we selected a NIL containing JU751 sequence through most of the chromosome II QTL (NIC1701) and injected sgRNAs (Synthego Corp.) to induce a double cut around the insertion site in the *lag-2* promoter (Figure S2, Table S13). We co-injected a single-stranded donor oligonucleotide to act as the repair template (Table S13). *dpy-10* was used in a co-CRISPR strategy according to[103]. Lines from separate injections containing successful replacements in *lag-2p* were identified by PCR genotyping of the deletion and sanger sequencing. These lines were then crossed to JU1200 to segregate away the chromosome II containing JU751 sequence to generate lines containing both the JU751 version of the chromosome II QTL and the *lag-2p(cgb1007)* deletion (NIC1713, NIC1714, NIC1715) as well as a line containing only the *lag-2p(cgb1007)* deletion in the JU1200 background (NIC1720). To replace the ancestral *lag-2p* deletion sequence (*cgb1008*) in the JU751 background, we selected a NIL containing JU1200 sequence in the chromosome II QTL (NIC1672) and injected guide RNAs (Synthego Corp.) (Table S13) to induce a double cut around the insertion site. We co-injected a double-stranded PCR product containing the ancestral (JU1200) sequence with *lag-2p(cgb1008)* to act as the repair template (Table S13). *dpy-10* was used in a co-CRISPR strategy according to[103]. Lines from separate injections containing successful replacements were identified by PCR genotyping of *lag-2p(cgb1008)* and Sanger sequencing. These lines were then crossed to JU751 to segregate away the chromosome II containing JU1200 sequence, leaving us with lines containing both the JU1200 version of the chromosome II QTL and *lag-2p(cgb1008)* (NIC1716, NIC1717, NIC1719) as well as lines containing only *lag-2p(cgb1007)* in the JU751 background (NIC1723, NIC1724, NIC1725). For a table of all lines created and genotypes, see Table S14.

Measurement of lag-2 transcripts via smFISH

Worms were bleach synchronized as above and grown at 20°C until the appropriate developmental stage. Worms were then washed off plates and fixed in 1mL fresh fixative (4% formaldehyde in PBS) for 40 min. Worms were washed twice in PBS, resuspended in 1mL 70% ethanol, and stored at 4°C for several days. A *lag-2* RNA probe set (Barkoulas et al. 2013) coupled to AF594 (Custom Stellaris Fish Probes, Biosearch Tech, Teddington UK) was resuspended in RNase-free TE buffer (pH8) to make a 100µM stock then diluted 1/30 (working solution) in RNase-free water. Fixed worms were washed 3 min in 1mL wash solution (10% deionized formamide and 2x Saline Sodium Citrate buffer (Ambion) in RNase-free water). Worms were then resuspended in 100µL hybridization solution (10% formamide, 10% dextran sulfate, 2x SSC) + 1 µL of the *lag-2* probe working solution and incubated in the dark at 30°C overnight. The following day, samples were rinsed, washed 30 min at 30°C in wash solution, and stained 30 min at 30°C

in 1mL wash solution + DAPI (7.5 µg/mL final, Sigma). Finally, samples were washed twice in PBS and mounted on glass slides in Prolong diamond antifade mounting medium (Eugene, OR). Worms were imaged under epifluorescence on an inverted Zeiss Z.1 microscope (RRID:SCR_020919) with a 100x oil immersion objective. The same illumination and exposure settings (Zen 3.2 Blue Edition software) were used for all samples. Z-stacks were taken through the DTC with a step size of 0.4µm and fluorescent puncta were quantified by hand using FIJI software (NIH, Bethesda, MD, http://rsb.info.nih.gov/ij/)

Quantification and statistical analysis

Statistical analyses were performed using R Statistical Software[104] (R version 4.2.0, RStudio 2022.02.3 build 492, RRID:SCR_001905) using generalized linear mixed models. Data were fitted to either gaussian or negative binomial (nbinom2) models using the glmmTMB package v. 1.1.3[105]. Residual diagnostics were performed using the DHARMa package v. 0.4.5 (RRID:SCR_022136) according to the developer's guidelines[106]. When model selection was warranted, the Bayesian information criterion (BIC) was used to select the optimal model. The emmeans package v. 1.7.4-1 (RRID:SCR_018734) was used to calculate model estimated marginal means, standard errors, and Tukey-corrected p-values for pairwise contrasts[107]. For model fitting of the interaction data set corresponding to Figure 6, D^2 was calculated using the modEvA package v. 3.0[77]. Specific details of each data analysis are described in the supplemental table legends, which display the statistical results (Tables S1-S12). Other R packages used for data manipulation and plotting included tidyverse v. 1.3.1[108] (RRID:SCR_019186), MASS v. 7.3-57[109] (RRID:SCR_019125), ggbeeswarm v. 0.6.0[110], rnaturalearth and rnaturalearthdata v. 0.1.0[111], rgeos v. 0.5-9[112], and sf v. 1.0-7[113].

References

1. Morrison, S.J., and Spradling, A.C. (2008). Stem Cells and Niches: Mechanisms That Promote Stem Cell Maintenance throughout Life. Cell *132*, 598–611. 10.1016/j.cell.2008.01.038.

2. Phillips, P.C. (2008). Epistasis - The essential role of gene interactions in the structure and evolution of genetic systems. Nat. Rev. Genet. *9*, 855–867. 10.1038/nrg2452.

3. Boyle, E.A., Li, Y.I., and Pritchard, J.K. (2017). An Expanded View of Complex Traits: From Polygenic to Omnigenic. Cell *169*, 1177–1186. 10.1016/j.cell.2017.05.038.

4. Campbell, R.F., McGrath, P.T., and Paaby, A.B. (2018). Analysis of Epistasis in Natural Traits Using Model Organisms. Trends Genet. *34*, 883–898. 10.1016/J.TIG.2018.08.002.

5. Jakobson, C.M., and Jarosz, D.F. (2020). What Has a Century of Quantitative Genetics Taught Us about Nature's Genetic Tool Kit? Annu. Rev. Genet. *54*, 439–464. 10.1146/ANNUREV-GENET-021920-102037.

6. Mackay, T.F.C. (2014). Epistasis and quantitative traits: using model organisms to study gene–gene interactions. Nat. Rev. Genet. *15*, 22–33. 10.1038/nrg3627.

7. Sackton, T.B., and Hartl, D.L. (2016). Genotypic Context and Epistasis in Individuals and Populations. Cell *166*, 279–287. 10.1016/j.cell.2016.06.047.

8. Weinreich, D.M., Lan, Y., Wylie, C.S., and Heckendorn, R.B. (2013). Should evolutionary geneticists worry about higher-order epistasis? Curr. Opin. Genet. Dev. *23*, 700–707. 10.1016/j.gde.2013.10.007.

9. Greene, J.S., Dobosiewicz, M., Butcher, R.A., McGrath, P.T., and Bargmann, C.I. (2016). Regulatory changes in two chemoreceptor genes contribute to a Caenorhabditis elegans QTL for foraging behavior. eLife *5*, e21454. 10.7554/eLife.21454.

10. Large, E.E., Padmanabhan, R., Watkins, K.L., Campbell, R.F., Xu, W., and McGrath, P.T. (2017). Modeling of a negative feedback mechanism explains antagonistic pleiotropy in reproduction in domesticated Caenorhabditis elegans strains. PLOS Genet. *13*, e1006769. 10.1371/journal.pgen.1006769.

11. Lee, J.T., Taylor, M.B., Shen, A., and Ehrenreich, I.M. (2016). Multi-locus Genotypes Underlying Temperature Sensitivity in a Mutationally Induced Trait. PLOS Genet. *12*, e1005929. 10.1371/journal.pgen.1005929.

12. Schweizer, G., and Wagner, A. (2020). Genotype networks of 80 quantitative Arabidopsis thaliana phenotypes reveal phenotypic evolvability despite pervasive epistasis. PLOS Comput. Biol. *16*, e1008082. 10.1371/journal.pcbi.1008082.

13. Taylor, M.B., and Ehrenreich, I.M. (2015). Higher-order genetic interactions and their contribution to complex traits. Trends Genet. *31*, 34–40. 10.1016/j.tig.2014.09.001.

14. Taylor, M.B., and Ehrenreich, I.M. (2014). Genetic Interactions Involving Five or More Genes Contribute to a Complex Trait in Yeast. PLOS Genet. *10*, e1004324. 10.1371/journal.pgen.1004324.

15. Vanhaeren, H., Gonzalez, N., Coppens, F., De Milde, L., Van Daele, T., Vermeersch, M., Eloy, N.B., Storme, V., and Inzé, D. (2014). Combining growth-promoting genes leads to positive epistasis in Arabidopsis thaliana. eLife *3*, e02252. 10.7554/eLife.02252.

16. Barkoulas, M., van Zon, J.S., Milloz, J., van Oudenaarden, A., and Félix, M.-A. (2013). Robustness and Epistasis in the C. elegans Vulval Signaling Network Revealed by Pathway Dosage Modulation. Dev. Cell *24*, 64–75. 10.1016/j.devcel.2012.12.001.

17. Hubbard, E.J.A., and Schedl, T. (2019). Biology of the *Caenorhabditis elegans* Germline Stem Cell System. Genetics *213*, 1145–1188. 10.1534/genetics.119.300238.

18. Laws, K.M., and Drummond-Barbosa, D. (2017). Control of Germline Stem Cell Lineages by Diet and Physiology. In Signaling-Mediated Control of Cell Division : From Oogenesis to Oocyte-to-Embryo Development, S. Arur, ed. (Springer International Publishing), pp. 67–99. 10.1007/978-3-319-44820-6_3.

19. Duveau, F., and Félix, M.-A. (2012). Role of Pleiotropy in the Evolution of a Cryptic Developmental Variation in Caenorhabditis elegans. PLOS Biol. *10*, e1001230. 10.1371/journal.pbio.1001230.

20. Agata, K., Nakajima, E., Funayama, N., Shibata, N., Saito, Y., and Umesono, Y. (2006). Two different evolutionary origins of stem cell systems and their molecular basis. Semin. Cell Dev. Biol. *17*, 503–509. 10.1016/j.semcdb.2006.05.004.

21. Gibson, G., and Hogness, D.S. (1996). Effect of Polymorphism in the Drosophila Regulatory Gene Ultrabithorax on Homeotic Stability. Science *271*, 200–203. 10.1126/science.271.5246.200.

22. Extavour, C.G., and Akam, M. (2003). Mechanisms of germ cell specification across the metazoans: epigenesis and preformation. Development *130*, 5869–5884. 10.1242/dev.00804.

23. Huang, X., Effgen, S., Meyer, R.C., Theres, K., and Koornneef, M. (2012). Epistatic Natural Allelic Variation Reveals a Function of AGAMOUS-LIKE6 in Axillary Bud Formation in Arabidopsis. Plant Cell *24*, 2364–2379. 10.1105/tpc.112.099168.

24. Lehmann, R. (2012). Germline Stem Cells: Origin and Destiny. Cell Stem Cell *10*, 729–739. 10.1016/j.stem.2012.05.016.

25. Koneru, S.L., Hintze, M., Katsanos, D., and Barkoulas, M. (2021). Cryptic genetic variation in a heat shock protein modifies the outcome of a mutation affecting epidermal stem cell development in C. elegans. Nat. Commun. *12*, 3263. 10.1038/s41467-021-23567-1.

26. Karp, X., and Greenwald, I. (2003). Post-transcriptional regulation of the E/Daughterless ortholog HLH-2, negative feedback, and birth order bias during the AC/VU decision in C. elegans. Genes Dev. *17*, 3100–3111. 10.1101/gad.1160803.

27. Paaby, A.B., White, A.G., Riccardi, D.D., Gunsalus, K.C., Piano, F., and Rockman, M.V. (2015). Wild worm embryogenesis harbors ubiquitous polygenic modifier variation. eLife *4*, e09178. 10.7554/eLife.09178.

28. Kocsisova, Z., Bagatelas, E.D., Santiago-Borges, J., Lei, H.C., Egan, B.M., Mosley, M.C., Schneider, D.L., Schedl, T., and Kornfeld, K. (2022). Notch signaling in germ line stem cells controls reproductive aging in C. elegans. 2022.03.04.482923. 10.1101/2022.03.04.482923.

29. Steiner, C.C., Weber, J.N., and Hoekstra, H.E. (2007). Adaptive Variation in Beach Mice Produced by Two Interacting Pigmentation Genes. PLOS Biol. *5*, e219. 10.1371/journal.pbio.0050219.

30. Poullet, N., Vielle, A., Gimond, C., Ferrari, C., and Braendle, C. (2015). Evolutionarily divergent thermal sensitivity of germline development and fertility in hermaphroditic Caenorhabditis nematodes. Evol. Dev. *17*, 380–397. 10.1111/ede.12170.

31. Vonesch, S.C., Lamparter, D., Mackay, T.F.C., Bergmann, S., and Hafen, E. (2016). Genome-Wide Analysis Reveals Novel Regulators of Growth in Drosophila melanogaster. PLOS Genet. *12*, e1005616. 10.1371/journal.pgen.1005616.

32. Rudel, D., and Kimble, J. (2001). Conservation of glp-1 Regulation and Function in Nematodes. Genetics *157*, 639–654. 10.1093/genetics/157.2.639.

33. Toomey, M.E., and Frydman, H.M. (2014). Extreme Divergence of Wolbachia Tropism for the Stem-Cell-Niche in the Drosophila Testis. PLOS Pathog. *10*, e1004577. 10.1371/journal.ppat.1004577.

34. Bubnell, J.E., Ulbing, C.K.S., Fernandez Begne, P., and Aquadro, C.F. (2022). Functional Divergence of the bag-of-marbles Gene in the Drosophila melanogaster Species Group. Mol. Biol. Evol. *39*. 10.1093/molbev/msac137.

35. Choi, J.Y., and Aquadro, C.F. (2015). Molecular Evolution of Drosophila Germline Stem Cell and Neural Stem Cell Regulating Genes. Genome Biol. Evol. *7*, 3097–3114. 10.1093/gbe/evv207.

36. Flores, H.A., DuMont, V.L.B., Fatoo, A., Hubbard, D., Hijji, M., Barbash, D.A., and Aquadro, C.F. (2015). Adaptive Evolution of Genes Involved in the Regulation of Germline Stem Cells in Drosophila melanogaster and D. simulans. G3 GenesGenomesGenetics *5*, 583–592. 10.1534/g3.114.015875.

37. Crittenden, S.L., and Kimble, J. (2008). Analysis of the C. elegans Germline Stem Cell Region. In Germline Stem Cells Methods in Molecular Biology™., S. X. Hou and S. R. Singh, eds. (Humana Press), pp. 27–44. 10.1007/978-1-60327-214-8_2.

38. Kimble, J., and Crittenden, S.L. (2007). Controls of germline stem cells, entry into meiosis, and the sperm/oocyte decision in Caenorhabditis elegans. Annu. Rev. Cell Dev. Biol. *23*, 405–433. 10.1146/annurev.cellbio.23.090506.123326.

39. Austin, J., and Kimble, J. (1989). Transcript analysis of glp-1 and lin-12, homologous genes required for cell interactions during development of C. elegans. Cell *58*, 565–571. 10.1016/0092-8674(89)90437-6.

40. Berry, L.W., Westlund, B., and Schedl, T. (1997). Germ-line tumor formation caused by activation of glp-1, a Caenorhabditis elegans member of the Notch family of receptors. Development *124*, 925–936. 10.1242/dev.124.4.925.

41. Gao, D., and Kimble, J. (1995). APX-1 can substitute for its homolog LAG-2 to direct cell interactions throughout Caenorhabditis elegans development. Proc. Natl. Acad. Sci. *92*, 9839–9842. 10.1073/pnas.92.21.9839.

42. Henderson, S.T., Gao, D., Lambie, E.J., and Kimble, J. (1994). lag-2 may encode a signaling ligand for the GLP-1 and LIN-12 receptors of C. elegans. Dev. Camb. Engl. *120*, 2913–2924.

43. Nadarajan, S., Govindan, J.A., McGovern, M., Hubbard, E.J.A., and Greenstein, D. (2009). MSP and GLP-1/Notch signaling coordinately regulate actomyosin-dependent cytoplasmic streaming and oocyte growth in C. elegans. Dev. Camb. Engl. *136*, 2223–2234. 10.1242/dev.034603.

44. Tax, F.E., Yeargers, J.J., and Thomas, J.H. (1994). Sequence of C. elegans lag-2 reveals a cell-signalling domain shared with Delta and Serrate of Drosophila. Nature *368*, 150–154. 10.1038/368150a0.

45. Yochem, J., and Greenwald, I. (1989). glp-1 and lin-12, genes implicated in distinct cell-cell interactions in C. elegans, encode similar transmembrane proteins. Cell *58*, 553–563. 10.1016/0092-8674(89)90436-4.

46. Chen, J., Mohammad, A., Pazdernik, N., Huang, H., Bowman, B., Tycksen, E., and Schedl, T. (2020). GLP-1 Notch—LAG-1 CSL control of the germline stem cell fate is mediated by transcriptional targets lst-1 and sygl-1. PLOS Genet. *16*, e1008650. 10.1371/JOURNAL.PGEN.1008650.

47. Hansen, D., and Schedl, T. (2013). Stem Cell Proliferation Versus Meiotic Fate Decision in Caenorhabditis elegans. In Germ Cell Development in C. elegans Advances in Experimental Medicine and Biology., T. Schedl, ed. (Springer), pp. 71–99. 10.1007/978-1-4614-4015-4_4.

48. Haupt, K.A., Law, K.T., Enright, A.L., Kanzler, C.R., Shin, H., Wickens, M., and Kimble, J. (2020). A PUF Hub Drives Self-Renewal in Caenorhabditis elegans Germline Stem Cells. Genetics *214*, 147–161. 10.1534/GENETICS.119.302772.

49. Gopal, S., Amran, A., Elton, A., Ng, L., and Pocock, R. (2021). A somatic proteoglycan controls Notch-directed germ cell fate. Nat. Commun. *12*, 6708. 10.1038/s41467-021-27039-4.

50. Gordon, K. (2020). Recent Advances in the Genetic, Anatomical, and Environmental Regulation of the C. elegans Germ Line Progenitor Zone. J. Dev. Biol. *8*, 14. 10.3390/JDB8030014.

51. Killian, D.J., and Hubbard, E.J.A. (2005). Caenorhabditis elegans germline patterning requires coordinated development of the somatic gonadal sheath and the germ line. Dev. Biol. *279*, 322–335. 10.1016/j.ydbio.2004.12.021.

52. Li, X., Singh, N., Miller, C., Washington, I., Sosseh, B., and Gordon, K.L. (2022). The C. elegans gonadal sheath Sh1 cells extend asymmetrically over a differentiating germ cell population in the proliferative zone. eLife *11*, e75497. 10.7554/eLife.75497.

53. McCarter, J., Bartlett, B., Dang, T., and Schedl, T. (1997). Soma–Germ Cell Interactions in Caenorhabditis elegans: Multiple Events of Hermaphrodite Germline Development Require the Somatic Sheath and Spermathecal Lineages. Dev. Biol. *181*, 121–143. 10.1006/dbio.1996.8429.

54. Starich, T.A., Hall, D.H., and Greenstein, D. (2014). Two Classes of Gap Junction Channels Mediate Soma-Germline Interactions Essential for Germline Proliferation and Gametogenesis in Caenorhabditis elegans. Genetics *198*, 1127–1153. 10.1534/genetics.114.168815.

55. Tolkin, T., and Hubbard, E.J.A. (2021). Germline Stem and Progenitor Cell Aging in C. elegans. Front. Cell Dev. Biol. *9*, 699671. 10.3389/fcell.2021.699671.

56. Angelo, G., and Van Gilst, M.R. (2009). Starvation Protects Germline Stem Cells and Extends Reproductive Longevity in C. elegans. Science *326*, 954–958. 10.1126/science.1178343.

57. Aprison, E.Z., and Ruvinsky, I. (2016). Sexually Antagonistic Male Signals Manipulate Germline and Soma of C. elegans Hermaphrodites. Curr. Biol. *26*, 2827–2833. 10.1016/j.cub.2016.08.024.

58. Cinquin, A., Chiang, M., Paz, A., Hallman, S., Yuan, O., Vysniauskaite, I., Fowlkes, C.C., and Cinquin, O. (2016). Intermittent Stem Cell Cycling Balances Self-Renewal and Senescence of the C. elegans Germ Line. PLoS Genet. *12*, e1005985. 10.1371/journal.pgen.1005985.

59. Seidel, H.S., and Kimble, J. (2015). Cell-cycle quiescence maintains Caenorhabditis elegans germline stem cells independent of GLP-1/Notch. eLife *4*, e10832. 10.7554/eLife.10832.

60. Sowa, J.N., Mutlu, A.S., Xia, F., and Wang, M.C. (2015). Olfaction Modulates Reproductive Plasticity through Neuroendocrine Signaling in Caenorhabditis elegans. Curr. Biol. *25*, 2284–2289. 10.1016/j.cub.2015.07.023.

61. Dalfó, D., Michaelson, D., and Hubbard, E.J.A. (2012). Sensory Regulation of the C. elegans Germline through TGF-β-Dependent Signaling in the Niche. Curr. Biol. *22*, 712–719. 10.1016/j.cub.2012.02.064.

62. Hubbard, E.J.A., Korta, D.Z., and Dalfó, D. (2013). Physiological Control of Germline Development. In Germ Cell Development in C. elegans Advances in Experimental Medicine and Biology., T. Schedl, ed. (Springer), pp. 101–131. 10.1007/978-1-4614-4015-4_5.

63. Korta, D.Z., Tuck, S., and Hubbard, E.J.A. (2012). S6K links cell fate, cell cycle and nutrient response in C. elegans germline stem/progenitor cells. Development *139*, 859–870. 10.1242/dev.074047.

64. Michaelson, D., Korta, D.Z., Capua, Y., and Hubbard, E.J.A. (2010). Insulin signaling promotes germline proliferation in C. elegans. Development *137*, 671–680. 10.1242/dev.042523.

65. Pekar, O., Ow, M.C., Hui, K.Y., Noyes, M.B., Hall, S.E., and Hubbard, E.J.A. (2017). Linking the environment, DAF-7/TGFβ signaling and LAG-2/DSL ligand expression in the germline stem cell niche. Dev. Camb. Engl. *144*, 2896–2906. 10.1242/dev.147660.

66. Rashid, S., Wong, C., and Roy, R. (2021). Developmental plasticity and the response to nutrient stress in Caenorhabditis elegans. Dev. Biol. *475*, 265–276. 10.1016/j.ydbio.2021.01.015.

67. Thondamal, M., Witting, M., Schmitt-Kopplin, P., and Aguilaniu, H. (2014). Steroid hormone signalling links reproduction to lifespan in dietary-restricted Caenorhabditis elegans. Nat. Commun. *5*, 4879. 10.1038/ncomms5879.

68. Poullet, N., Vielle, A., Gimond, C., Carvalho, S., Teotónio, H., and Braendle, C. (2016). Complex heterochrony underlies the evolution of Caenorhabditis elegans hermaphrodite sex allocation. Evolution *70*, 2357–2369. 10.1111/evo.13032.

69. Cook, D.E., Zdraljevic, S., Roberts, J.P., and Andersen, E.C. (2017). CeNDR, the Caenorhabditis elegans natural diversity resource. Nucleic Acids Res. *45*, D650–D657. 10.1093/nar/gkw893.

70. Vigne, P., Gimond, C., Ferrari, C., Vielle, A., Hallin, J., Pino-Querido, A., Mouridi, S.E., Mignerot, L., Frøkjær-Jensen, C., Boulin, T., et al. (2021). A single-nucleotide change underlies the genetic assimilation of a plastic trait. Sci. Adv. *7*. 10.1126/SCIADV.ABD9941.

71. Broman, K.W., and Saunak, S. (2009). A Guide to QTL Mapping with R/qtl (Springer Science+Business Media, LLC).

72. Chesney, M.A., Lam, N., Morgan, D.E., Phillips, B.T., and Kimble, J. (2009). C. elegans HLH-2/E/Daughterless controls key regulatory cells during gonadogenesis. Dev. Biol. *331*, 14–25. 10.1016/j.ydbio.2009.04.015.

73. Lee, D., Zdraljevic, S., Stevens, L., Wang, Y., Tanny, R.E., Crombie, T.A., Cook, D.E., Webster, A.K., Chirakar, R., Baugh, L.R., et al. (2021). Balancing selection maintains hyper-divergent haplotypes in Caenorhabditis elegans. Nat. Ecol. Evol. *5*, 794–807. 10.1038/s41559-021-01435-x.

74. Barrière, A., and Félix, M.-A. (2007). Temporal Dynamics and Linkage Disequilibrium in Natural Caenorhabditis elegans Populations. Genetics *176*, 999–1011. 10.1534/genetics.106.067223.

75. Raj, A., Rifkin, S.A., Andersen, E., and van Oudenaarden, A. (2010). Variability in gene expression underlies incomplete penetrance. Nature *463*, 913–918. 10.1038/nature08781.

76. Raj, A., van den Bogaard, P., Rifkin, S.A., van Oudenaarden, A., and Tyagi, S. (2008). Imaging individual mRNA molecules using multiple singly labeled probes. Nat. Methods *5*, 877–879. 10.1038/nmeth.1253.

77. Márcia Barbosa, A., Real, R., Muñoz, A.-R., and Brown, J.A. (2013). New measures for assessing model equilibrium and prediction mismatch in species distribution models. Divers. Distrib. *19*, 1333–1338. 10.1111/ddi.12100.

78. Bernstein, M.R., Zdraljevic, S., Andersen, E.C., and Rockman, M.V. (2019). Tightly linked antagonistic-effect loci underlie polygenic phenotypic variation in *C. elegans*. Evol. Lett. *3*, 462–473. 10.1002/evl3.139.

79. Cheverud, J.M., and Routman, E.J. (1995). Epistasis and its contribution to genetic variance components. Genetics *139*, 1455–1461. 10.1093/genetics/139.3.1455.

80. Falconer, D.S. (1996). Introduction to Quantitative Genetics (Pearson Education).

81. Forsberg, S.K.G., Bloom, J.S., Sadhu, M.J., Kruglyak, L., and Carlborg, Ö. (2017). Accounting for genetic interactions improves modeling of individual quantitative trait phenotypes in yeast. Nat. Genet. *49*, 497–503. 10.1038/ng.3800.

82. Hill, W.G., Goddard, M.E., and Visscher, P.M. (2008). Data and Theory Point to Mainly Additive Genetic Variance for Complex Traits. PLOS Genet. *4*, e1000008. 10.1371/journal.pgen.1000008.

83. Huang, W., and Mackay, T.F.C. (2016). The Genetic Architecture of Quantitative Traits Cannot Be Inferred from Variance Component Analysis. PLOS Genet. *12*, e1006421. 10.1371/journal.pgen.1006421.

84. Lachowiec, J., Shen, X., Queitsch, C., and Carlborg, Ö. (2015). A Genome-Wide Association Analysis Reveals Epistatic Cancellation of Additive Genetic Variance for Root Length in Arabidopsis thaliana. PLOS Genet. *11*, e1005541. 10.1371/journal.pgen.1005541.

85. Mäki-Tanila, A., and Hill, W.G. (2014). Influence of Gene Interaction on Complex Trait Variation with Multilocus Models. Genetics *198*, 355–367. 10.1534/genetics.114.165282.

86. Monnahan, P.J., and Kelly, J.K. (2015). Epistasis Is a Major Determinant of the Additive Genetic Variance in Mimulus guttatus. PLOS Genet. *11*, e1005201. 10.1371/journal.pgen.1005201.

87. Aprison, E.Z., Dzitoyeva, S., Angeles-Albores, D., and Ruvinsky, I. (2022). A male pheromone that improves the quality of the oogenic germline. Proc. Natl. Acad. Sci. *119*, e2015576119. 10.1073/pnas.2015576119.

88. Kocsisova, Z., Kornfeld, K., and Schedl, T. (2019). Rapid population-wide declines in stem cell number and activity during reproductive aging in C. elegans. Dev. Camb. Engl. *146*, dev173195. 10.1242/dev.173195.

89. Cutter, A.D., Dey, A., and Murray, R.L. (2009). Evolution of the Caenorhabditis elegans Genome. Mol. Biol. Evol. *26*, 1199–1234. 10.1093/molbev/msp048.

90. Noble, L.M., Yuen, J., Stevens, L., Moya, N., Persaud, R., Moscatelli, M., Jackson, J.L., Zhang, G., Chitrakar, R., Baugh, L.R., et al. (2021). Selfing is the safest sex for Caenorhabditis tropicalis. eLife *10*, e62587. 10.7554/eLife.62587.

91. Rockman, M.V., Skrovanek, S.S., and Kruglyak, L. (2010). Selection at Linked Sites Shapes Heritable Phenotypic Variation in C. elegans. Science *330*, 372–376. 10.1126/science.1194208.

92. Ben-David, E., Pliota, P., Widen, S.A., Koreshova, A., Lemus-Vergara, T., Verpukhovskiy, P., Mandali, S., Braendle, C., Burga, A., and Kruglyak, L. (2021). Ubiquitous Selfish Toxin-Antidote Elements in Caenorhabditis Species. Curr. Biol. *31*, 990-1001.e5. 10.1016/j.cub.2020.12.013.

93. Dolgin, E.S., Charlesworth, B., Baird, S.E., and Cutter, A.D. (2007). Inbreeding and Outbreeding Depression in Caenorhabditis Nematodes. Evolution *61*, 1339–1352. 10.1111/j.1558-5646.2007.00118.x.

94. Gimond, C., Jovelin, R., Han, S., Ferrari, C., Cutter, A.D., and Braendle, C. (2013). Outbreeding Depression with Low Genetic Variation in Selfing Caenorhabditis Nematodes. Evolution *67*, 3087–3101. 10.1111/evo.12203.

95. Seidel, H.S., Rockman, M.V., and Kruglyak, L. (2008). Widespread Genetic Incompatibility in C. Elegans Maintained by Balancing Selection. Science *319*, 589–594. 10.1126/science.1151107.

96. Chandler, C.H., Chari, S., Kowalski, A., Choi, L., Tack, D., DeNieu, M., Pitchers, W., Sonnenschein, A., Marvin, L., Hummel, K., et al. (2017). How well do you know your mutation? Complex effects of genetic background on expressivity, complementation, and ordering of allelic effects. PLOS Genet. *13*, e1007075. 10.1371/journal.pgen.1007075.

97. Gibson, G., and Dworkin, I. (2004). Uncovering cryptic genetic variation. Nat. Rev. Genet. *5*, 681–690. 10.1038/nrg1426.

98. Noble, L.M., Rockman, M.V., and Teotónio, H. (2021). Gene-level quantitative trait mapping in Caenorhabditis elegans. G3 GenesGenomesGenetics *11*, jkaa061. 10.1093/g3journal/jkaa061.

99. Brenner, S. (1974). The Genetics of Caenorhabditis elegans. Genetics *77*, 71–94. 10.1093/genetics/77.1.71.

100. Stiernagle, T. (2006). Maintenance of C. elegans. WormBook. 10.1895/wormbook.1.101.1.

101. Wood, W.B. (1988). Determination of Pattern and Fate in Early Embryos of Caenorhabditis elegans. In The Molecular Biology of Cell Determination and Cell Differentiation Developmental Biology., L. W. Browder, ed. (Springer US), pp. 57–78. 10.1007/978-1-4615-6817-9_2.

102. Billard, B., Vigne, P., and Braendle, C. (2020). A Natural Mutational Event Uncovers a Life History Trade-Off via Hormonal Pleiotropy. Curr. Biol. *30*, 4142-4154.e9. 10.1016/j.cub.2020.08.004.

103. Paix, A., Folkmann, A., Rasoloson, D., and Seydoux, G. (2015). High Efficiency, Homology-Directed Genome Editing in Caenorhabditis elegans Using CRISPR-Cas9 Ribonucleoprotein Complexes. Genetics *201*, 47–54. 10.1534/genetics.115.179382.

104. R Core Team (2021). R: A language and environment for staistical computing.

105. Brooks, M.E., Kristensen, K., van Benthem, K.J., Magnusson, A., Berg, C.W., Nielsen, A., Skaug, H.J., Machler, M., and Bolker, B.M. (2017). glmmTMB balances speed and flexibility among packages for zero-inflated generalized linear mixed modeling. R J. *9*, 378–400. 10.3929/ethz-b-000240890.

106. Hartig, F. (2022). DHARMa: Residual Diagnostics for Hierarchical (Multi-Level/Mixed) Regression Models.

107. Length, R. (2022). emmeans: Estimated Marginal Means, aka Least-Squares Means.

108. Wickham, H., Averick, M., Bryan, J., Chang, W., McGowan, L.D., François, R., Grolemund, G., Hayes, A., Henry, L., Hester, J., et al. (2019). Welcome to the Tidyverse. J. Open Source Softw. *4*, 1686. 10.21105/joss.01686.

109. Venables, W.N., Ripley, B.D., and Venables, W.N. (2002). Modern applied statistics with S Fourth. (Springer).

110. Clarke, E., and Sherrill-Mix, S. (2017). ggbeeswarm: Categorical Scatter (Violin Point) Plots. R package version 0.6.0.

111. South, A. (2022). rnaturalearth: World Map Data from Natural Earth. https://docs.ropensci.org/rnaturalearth.

112. Bivand, R., and Rundel, C. (2021). rgeos: Interface to Geometry Engine - Open Source ('GEOS'). https://r-forge.r-project.org/projects/rgeos/.

113. Pebesma, E. (2018). Simple Features for R: Standardized Support for Spatial Vector Data. R J. *10*, 439–446. 10.32614/RJ-2018-009.